ChemComm

ROYAL SOCIETY OF CHEMISTRY

COMMUNICATION

View Article Online
View Journal | View Issue

Open Access Article. Published on 29 September 2025. Downloaded on 10/29/2025 11:56:28 AM.
This article is licensed under a Creative Commons Attribution 3.0 Unported Licence.

Check for updates

Cite this: *Chem. Commun.*, 2025, **61**, 16950

Received 2nd September 2025,
Accepted 26th September 2025

DOI: 10.1039/d5cc05078b

rsc.li/chemcomm

Matrix-isolation IR spectra of halogen–P and halogen–π complexes of phosphines and iodotrifluoroethylene (C_2F_3I)

Malte Feßner, Elliot J. Tay, Corentin Grassin, Sven Reese and Christian Merten *

The C═C stretching mode of iodotrifluoroethylene (ITFE) serves as a marker for halogen-bonding (XB) interactions in complexes with phosphines. The formation of C–I···P XB-complexes becomes evident from a strong red-shift of this marker band. The formation of C–I···π bound clusters, which were kinetically trapped in the cryogenic environment, was confirmed by a slightly smaller red-shift of the marker band.

In its most general definition, a halogen bonding (XB) interaction[1–4] results from a net attraction between an electrophilic region of a halogen atom and a nucleophilic region in either the same or another molecule. In practice, halogen bonding donors are dihalogen compounds or haloorganics, and halogen bonding acceptors are entities that would also act as hydrogen bonding acceptors. The high directionality of XB interactions finds application in various fields, ranging from crystal engineering to catalysis[5,6] and supramolecular chemistry.[7–10] Among the most utilized structural motifs are C–X bonds (with X = Br, I) interacting with the nitrogen atoms of amines or the oxygens in carbonyl or ether groups. Halides,[11,12] selenium,[13,14] and sulfur[15] are also known to form halogen bonds.[16–20] Interestingly, although phosphines could also engage in XB interactions, examples in the literature are scarce. This lack of examples is due to the fact that the strongly polarizing phosphorus tends to abstract the halogen atom from the XB-donor,[21] resulting in the formation of a covalent P–X bond. Most C–X···P halogen bonds reported in the literature are thus reported in the solid state and investigated by means of X-ray crystallography or solid-state NMR spectroscopy.[16,22–24] Solely for the complex formed between triphenylphosphine and 1,3,5-trifluoro-2,4,6-triiodobenzene, not only the solid state but also a solution-phase identification based on ^{31}P-NMR was reported.[22]

The infrared (IR) spectroscopic characterization of such weakly bound C–X···P complexes in the solution phase is hampered not only because of the potential reactivity of the mixture, but also because they may compete with solute–solvent interactions. Furthermore, band shifts associated with the complexes may be very small, so that the spectra would only slightly differ from those of the single components. Consequently, the broad bands of the solution phase measurements simply prevent their identification. The technique of matrix isolation (MI) is well-established for the characterization of conformational equilibria and intermolecular interactions as well as for studies on reactive intermediates. It involves the separation of target compounds and complexes in solid inert gas matrices, which are obtained by spraying mixtures of the components and an inert gas onto a spectroscopic window. The window is held at a temperature markedly below the melting point of the host gas (typically ∼15–20 K), so that the arriving species are immediately frozen out. If the solid matrix is subsequently slightly warmed (annealing), small guest molecules can diffuse through the matrix and form clusters. As the rigid environment prevents any large amplitude structural rearrangements of larger guest molecules, the diffusion process may not only yield the thermodynamically most favourable complexes. In fact, high-energy structures may become kinetically trapped.

Using matrix isolation and other cryogenic sampling techniques, the C═C stretching vibration of iodotrifluoroethylene (ITFE) has been identified as a particularly sensitive probe for XB interactions. As shown by Herrebout *et al.* in cryosolution experiments, *i.e.*, when using liquefied rare gases as solvents,[25,26] XB interactions of ITFE with amines lead to a strong shift of 10–15 cm^{-1}. For ferrocene and *N*,*N*-dimethyl ferrocenyl amine, we recently reported that ITFE also interacts with the π-faces of cyclopentadienyl giving C–I···π bound clusters under MI conditions.[27] Our detailed MI-IR study on ITFE itself revealed the presence of a particularly stable matrix site in argon, which persists when the matrix is annealed.[28] We subsequently identified *para*-hydrogen as an ideal environment to study complexes of ITFE, as no self-aggregation was observable under typical deposition conditions.[28] Notably, we also demonstrated that strong contributions of combination modes

Ruhr-Universität Bochum, Fakultät für Chemie und Biochemie, Organische Chemie II, Universitätsstraße 150, 44801 Bochum, Germany. E-mail: christian.merten@ruhr-uni-bochum.de; Web: https://www.mertenlab.de

 This journal is © The Royal Society of Chemistry 2025

Open Access Article. Published on 29 September 2025. Downloaded on 10/29/2025 11:56:28 AM.
This article is licensed under a Creative Commons Attribution 3.0 Unported Licence.

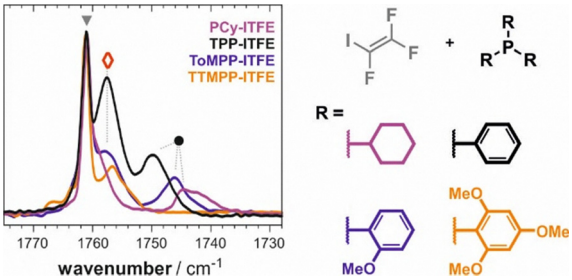

Fig. 1 Experimental spectra of **ITFE** co-deposited with **PCy$_3$**, **TPP**, **ToMPP** and **TTMPP** in a *para*-hydrogen matrix at 4 K in the range of the C═C stretching band of ITFE. The spectra are normalized to the band of monomeric ITFE (▼). Bands arising from the complexes of the phosphines with ITFE are marked (●) and (◊). The full fingerprint range is presented in the SI.

and overtones complicate the analysis of the spectral regions around the other fundamental modes of ITFE.

It was envisioned that ITFE could be the ideal probe to also characterize neutral XB interactions with phosphines. For the present study, we thus recorded the MI-IR spectra of **ITFE** co-deposited with tricyclohexyl phosphine (**PCy$_3$**), triphenyl phosphine (**TPP**), tris(*o*-methoxy phenyl)phosphine (**ToMPP**), and tris(2,4,6-trimethoxy phenyl)phosphine (**TTMPP**). In addition to the C═C stretching band of monomeric **ITFE**, which is observed at 1761.3 cm^{-1} (▼, Fig. 1) in the pH$_2$ matrix, the spectra of all four investigated systems showed additional bands in the C═C stretching regions indicative of complex formation during the deposition process. For three systems, a strongly red-shifted band (●) was observed (1744.6 cm^{-1} for **PCy$_3$**, 1746.1 cm^{-1} for **ToMPP**, 1749.8 cm^{-1} for **TPP**), which was apparently absent in the spectrum of **TTMPP**. Another sharp band (◊) was found at 1757.6 for **TPP** and **ToMPP**, and at 1756.7 cm^{-1} for **TTMPP**, respectively. In the same range, there is only a shoulder to the monomeric **ITFE** band visible near 1759 cm^{-1} for **ITFE-PCy$_3$**. In the remaining fingerprint region, new bands could also be observed near some of the other strong fundamental modes of ITFE (*cf.* Fig. S1). Most notably, very characteristic new bands occurred around the in-phase C–F stretching mode of **ITFE** ($\nu_{CF2,ip}$, 1004.5 cm^{-1}). In all four spectra, a new band at ∼1002.3 cm^{-1} likely corresponds to the same species as the weakly shifted C═C stretching modes (◊). Further red-shifted bands occurred at 993.1 cm^{-1} for **ITFE-PCy$_3$** and 994.4 cm^{-1} for **ITFE-ToMPP**. There is likely also a band present at ∼997 cm^{-1} in the spectrum of **ITFE-TPP**, yet this range is overlapped with a band of **TPP** itself. For **TTMPP**, however, a similar band is clearly absent. The observed strongly shifted bands of $\nu_{CF2,ip}$ follow the same trend as the strongly shifted C═C stretching bands (●), suggesting that these bands belong to the same species. It is further noteworthy, that no changes in the bands of the phosphines were observed as the XB-acceptors were deposited in large excess. Generally, the same trend can be observed in the Ar-matrix after deposition (*cf.* Fig. S2) and annealing of the Ar-matrices further intensified the complex bands.

For the computational analysis of **ITFE-PCy$_3$**, three types of intermolecular interactions were considered (Fig. 2). The C–I···P XB interaction was found to be the most preferred at the utilized levels of theory, *i.e.*, at the B3LYP-d3bj[29] and revDSD-PBEP86-d3bj[30] levels with the def2TZVP basis. More than 3.5 kcal mol^{-1} less favourable is the second complex structure, which is best described as cooperative P···π/C–H···F interactions. Another 1.6–1.8 kcal mol^{-1} higher in energy is the third structure obtained for **ITFE-PCy$_3$**, which is stabilized by C–H···π interactions between a cyclohexyl ring and the ITFE molecule located above the ring. A structure with C–H···I interaction could not be obtained. Based on the computed harmonic IR spectra of these three structures, the strongly shifted band at 1744.6 cm^{-1} (●) could unambiguously be assigned to the C–I···P XB-complex ($\Delta\nu_{exp}$ = 16.7 cm^{-1}; $\Delta\nu_{B3LYP}$ = 18.6 cm^{-1}; $\Delta\nu_{revDSD}$ = 14.1 cm^{-1}). The calculations further suggested that the C–H···π interactions cause a very small red-shift of the C═C stretching band ($\Delta\nu_{exp}$ = ∼2 cm^{-1}; $\Delta\nu_{B3LYP}$ = 0.3 cm^{-1}; $\Delta\nu_{revDSD}$ = 0.5 cm^{-1}), while the π–P/C–H···F interactions result in a blue-shift. Consistent also with the predicted shifts of the other fundamental modes of **ITFE** (*cf.* Fig. S3), the experimentally observed shoulder (◊) in the **PCy$_3$-ITFE** spectrum was thus assigned to a kinetically trapped C–H···π complex and it was concluded that the π···P/C–H···F complex is not formed under MI conditions.

In the screening for complex structures of **TPP-ITFE**, we also found three general binding motifs. In addition to the C–I···P

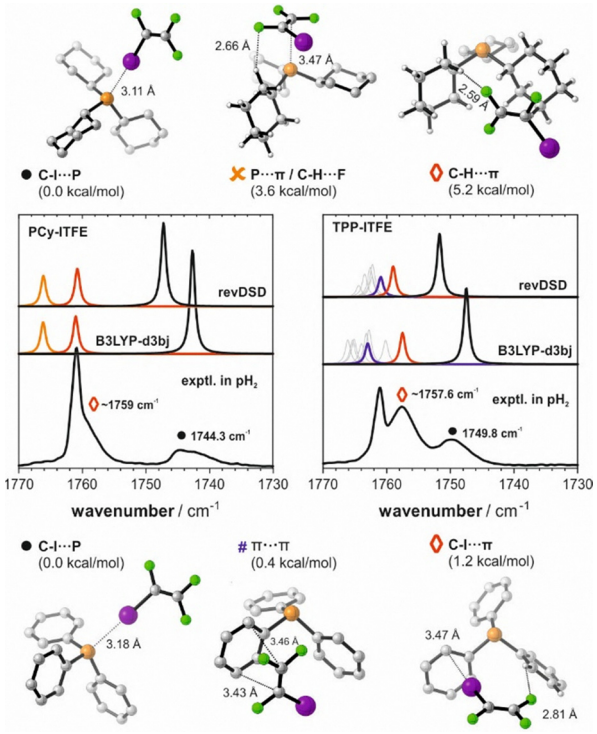

Fig. 2 Comparison of the computed IR spectra with the experimental spectra of **ITFE** and its complexes with **PCy$_3$** (left) and **TPP** (right) recorded in the pH$_2$ matrix at 4 K. The analytically relevant section around the C═C stretching mode of **ITFE** is shown, as the remaining fingerprint region is of little diagnostic value. The figure also shows representative complex structures of **PCy$_3$-ITFE** (top) and **TPP-ITFE** (bottom), with bond lengths and relative ΔE_{ZPC} obtained at the revDSD-PBEP86-d3bj/def2TZVP level. The grey spectra in the figure of **TPP-ITFE** correspond to other π···π structures.

Open Access Article. Published on 29 September 2025. Downloaded on 10/29/2025 11:56:28 AM.
This article is licensed under a Creative Commons Attribution 3.0 Unported Licence.

XB-structure, **ITFE** can interact with the π-faces of the aryl rings forming either C–I···π or π···π complexes (Fig. 2, bottom). The C–I···P complex was again found to be the lowest energy structure, followed by several π···π structures (ΔE_{B3LYP} = 1.1–1.7 kcal mol^{-1}, ΔE_{revDSD} = 0.4–0.7 kcal mol^{-1}, *cf.* Table S1) and the C–I···π complex (ΔE_{B3LYP} = 2.0 kcal mol^{-1}, ΔE_{revDSD} = 1.2 kcal mol^{-1}). The computed vibrational spectra allowed for the unambiguous analysis of the experimental IR spectra of **TPP-ITFE**. The C═C stretching band in the C–I···P XB-complex again showed the largest shift (*cf.* Fig. 2), which well-matched in magnitude with the experimentally observed values ($\Delta\nu_{exp}$ = 11.8 cm^{-1}; $\Delta\nu_{B3LYP}$ = 13.8 cm^{-1}; $\Delta\nu_{revDSD}$ = 9.6 cm^{-1}). Likewise, the strong band at 1749.8 cm^{-1} (◊) could directly be assigned to the C–I···π complex ($\Delta\nu_{exp}$ = 3.7 cm^{-1}; $\Delta\nu_{B3LYP}$ = 3.8 cm^{-1}; $\Delta\nu_{revDSD}$ = 2.3 cm^{-1}), as the π···π complexes are expected to be much closer to the ITFE monomer band. Again, the assignments were also consistent with the observed shifts in the spectral regions of the other fundamental modes of **ITFE** (*cf.* Fig. S4).

For the analysis of **ToMPP-ITFE** and **TTMPP-ITFE**, we focused on spectral calculations at the B3LYP-d3bj level of theory, as the increasing molecular size of the complexes made calculations at revDSD-PBEP86-d3bj not feasible anymore. In its lowest energy conformation, the three methoxy groups of **ToMPP** are oriented in the same direction, *i.e.*, pointing towards the lone pair of the central phosphorus.[31] Under solution phase conditions, a coordination to the lone pair typically leads to the rotation of one aryl unit to decrease steric repulsion (see crystal structures of **ToMPP**-BH_3[32] or RhCl (**ToMPP**)(1,5-cyclo-octadiene)[33] for examples). Under matrix isolation conditions, however, such a large amplitude motion required for this conformational change cannot take place. Hence, for the generation of **ToMPP-ITFE** structures, we assumed that the complex formation takes place solely with the lowest energy structure. Expectedly, the analysis of the IR spectrum of **ToMPP-ITFE** subsequently led to a very similar conclusion to that of **TPP-ITFE**, and it showed that C–I···P and C–I···π structures are present in the matrix (*cf.* Table S2 and Fig. S5).

Initially following the same approach as that of **ToMPP**, we computed **TTMPP-ITFE** complexes based on the crystal structure conformation.[34,35] Due to the steric crowding with two *ortho*-methoxy groups, **TTMPP** cannot adopt a symmetric propeller conformation with the three aryl rings being tilted in the same direction. Instead, one of the aryl rings arranges almost in plane with the lone pair of phosphorus. In a second low-energy structure of **TTMPP**, a methoxy group on the non-tilted aryl ring is rotated towards the phosphorus, which increases the steric shielding of the lone pair but lowers the zero-point corrected energy by about 0.2 kcal mol^{-1} (*cf.* Fig. 3 and Fig. S3). For both conformers of **TTMPP**, the C–I···P XB-complexes were found to be the most favourable complexes with **ITFE**. The shielding of the phosphorus with the methoxy group, however, introduced a drastic energy difference between the two C–I···P XB-complexes of 1.25 kcal mol^{-1}, clearly favouring the complex of the crystal structure-like conformer of **TTMPP** (*cf.* Fig. S6 for electrostatic potential maps). Notably, interactions with the methoxy oxygen

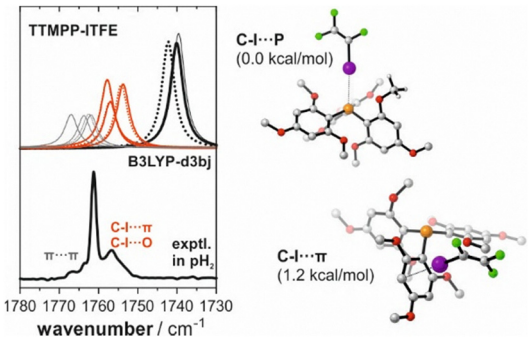

Fig. 3 Comparison of the computed spectra of **ITFE-TTMPP** complexes with the experimental spectra recorded in the *para*-hydrogen matrix at 4 K in the range of the C═C stretching band of **ITFE**. The dotted spectra correspond to structures of the second **TTMPP** conformation with the methoxy group rotated towards the phosphorus lone pair (*cf.* Table S3). The grey spectra in the figure correspond to π···π structures.

atoms are significantly less favoured than those with the phosphorus. Expectedly, the characteristic, strongly red-shifted band of the C═C stretching mode was predicted for both complexes, yet it is absent in the experiment. The C═C stretching bands of **ITFE** in the C–I···π structures coincided with those of the C–I···O complexes, which could both well explain the band at 1756.7 cm^{-1} (◊). The π···π complexes could explain the small features seen at the high-energy side of the C═C stretching band of **ITFE**.

From the computational analysis of the spectra, there is no apparent reason for the C–I···P XB-complexes being formed under matrix isolation only with **PCy$_3$**, **TPP** and **ToMPP**, but not with **TTMPP**. It confirmed the presence of higher energy complexes for all four phosphines, which are kinetically trapped and cannot rearrange towards the thermodynamically most preferred structures (*i.e.*, the C–I···P complexes). Notably, a comparison of the relative intensities of the diagnostic C═C stretching bands (● and ◊) suggested that the higher energy C–H···π and C–I···π states were the predominant species in the matrix. As the complex formation process under matrix isolation conditions is determined by diffusion processes within the deposited matrix, a mechanistic explanation for the lack of the C–I···P complex could be formulated. For the complex to form, **ITFE** must approach the phosphine at a suitable angle and ideally with the iodine first, and **ITFE** must have sufficient space around the phosphorus lone pair for it to move into a linear arrangement. With **TTMPP** being the sterically most demanding of the investigated phosphines based on the Tolman cone angles,[36] the chances for an encounter under these conditions are likely to be very limited. Instead, approaching **ITFE** molecules face the very attractive π-faces or slightly less preferable oxygen sites of the methoxy groups first and become kinetically trapped in the higher energy π···π, C–I···π or C–I···O states (*cf.* Fig. S6 for electrostatic potentials). For **PCy$_3$**, **TPP** and **ToMPP**, the lone pairs are more exposed to the matrix environment and the approach is not shielded by methoxy groups. Consequently, as the lone pair represents also the most electronegative site for **PCy$_3$** and **TTP**, the statistical

Open Access Article. Published on 29 September 2025. Downloaded on 10/29/2025 11:56:28 AM.
This article is licensed under a Creative Commons Attribution 3.0 Unported Licence.

Table 1 Comparison of the experimental band shift of the C═C stretching vibration ($\Delta\nu_{exp}$, cm^{-1}) with computed shifts ($\Delta\nu_{calc}$, cm^{-1}), C–I···P bond distances ($d_{C-I\cdots P}$, Å) and interaction energy ($\Delta E_{int} = E_{ZPC,complex} - E_{ZPC,phosphine} - E_{ZPC,ITFE}$; kcal mol^{-1})

			B3LYP-d3bj		revDSD-PBEp86-d3bj	
	$\Delta\nu_{exp}$	$\Delta\nu_{calc}$	$d_{C-I\cdots P}$	ΔE_{int}	$\Delta\nu_{calc}$	$d_{C-I\cdots P}$
PCy3-ITFE	16.7	18.6	3.11	−11.0	14.1	3.16
ToMPP-ITFE	15.2	17.4	3.14	−12.2	—	—
TPP-ITFE	11.8	13.8	3.18	−8.4	9.6	3.24
TTMPP-ITFE	—	21.3	3.11	−15.6	—	—

chance for the C–I···P XB-complex under MI conditions is notably increased.

The matrix isolation spectra presented in this study allow the key conclusion that phosphines can engage in C–I···P halogen bonding interactions. They do not allow the converse conclusion, *i.e.*, that **TTMPP** cannot form XB interaction through the phosphorus at all. Steric effects are likely to play a role in the complex formation process under matrix isolation conditions. Finally, it is interesting to note that there appears to be a certain correlation of the computed C–I···P bond distances in the ITFE-complexes of **PCy$_3$**, **TPP** and **ToMPP** with the frequency of the ITFE C═C stretching bands. Shorter distances lead to a stronger shift (*cf.* Table 1). However, when also considering the computed values for **TTMPP-ITFE**, it is not only the distance, but also secondary stabilizing interactions (*cf.* Fig. S7) that contribute to the shift of the C═C stretching band. Whether or not the position of the C═C stretching band has analytical value to compare XB interactions among different complexes needs to be explored in further detail in future studies.

We conclude this study by acknowledging financial support by the Deutsche Forschungsgemeinschaft (DFG, German Research Foundation) under Germany's Excellence Strategy (EXC-2033, project no. 390677874), through the Research Training Group "Confinement Controlled Chemistry" (GRK 2376, project no. 331085229) and a research project (ME 4267/6-1, project no. 418662566). Further financial support was provided by the Mercator Research Center Ruhr (MERCUR, Pr-2017-0018).

Conflicts of interest

There are no conflicts to declare.

Data availability

The data supporting this article have been included as part of the supplementary information (SI). Supplementary information: experimental and computational details, additional experimental and computed spectra, energies, electrostatic potential maps, NCI analysis. See DOI: **https://doi.org/10.1039/d5cc05078b**.

Notes and references

1 G. Cavallo, P. Metrangolo, R. Milani, T. Pilati, A. Priimagi, G. Resnati and G. Terraneo, *Chem. Rev.*, 2016, **116**, 2478–2601.
2 T. Clark, M. Hennemann, J. S. Murray and P. Politzer, *J. Mol. Model.*, 2007, **13**, 291–296.
3 M. Fourmigué, *Curr. Opin. Solid State Mater. Sci.*, 2009, **13**, 36–45.
4 M. Erdelyi, *Chem. Soc. Rev.*, 2012, **41**, 3547–3557.
5 S. H. Jungbauer, S. M. Walter, S. Schindler, L. Rout, F. Kniep and S. M. Huber, *Chem. Commun.*, 2014, **50**, 6281–6284.
6 R. L. Sutar, E. Engelage, R. Stoll and S. M. Huber, *Angew. Chem., Int. Ed.*, 2020, **59**, 6806–6810.
7 P. Metrangolo, F. Meyer, T. Pilati, G. Resnati and G. Terraneo, *Angew. Chem., Int. Ed.*, 2008, **47**, 6114–6127.
8 L. C. Gilday, S. W. Robinson, T. A. Barendt, M. J. Langton, B. R. Mullaney and P. D. Beer, *Chem. Rev.*, 2015, **115**, 7118–7195.
9 A. Brown and P. D. Beer, *Chem. Commun.*, 2016, **52**, 8645–8658.
10 J. Y. C. Lim, I. Marques, V. Félix and P. D. Beer, *Angew. Chem., Int. Ed.*, 2018, **57**, 584–588.
11 S. Triguero, R. Llusar, V. Polo and M. Fourmigué, *Cryst. Growth Des.*, 2008, **8**, 2241–2247.
12 M. G. Chudzinski, C. A. McClary and M. S. Taylor, *J. Am. Chem. Soc.*, 2011, **133**, 10559–10567.
13 M. Iwaoka, T. Katsuda, H. Komatsu and S. Tomoda, *J. Org. Chem.*, 2005, **70**, 321–327.
14 H. D. Arman, E. R. Rafferty, C. A. Bayse and W. T. Pennington, *Cryst. Growth Des.*, 2012, **12**, 4315–4323.
15 D. Hauchecorne, A. Moiana, B. J. van der Veken and W. A. Herrebout, *Phys. Chem. Chem. Phys.*, 2011, **13**, 10204–10213.
16 K. Lisac, F. Topić, M. Arhangelskis, S. Cepić, P. A. Julien, C. W. Nickels, A. J. Morris, T. Friščić and D. Cinčić, *Nat. Commun.*, 2019, **10**, 61.
17 M. V. Chernysheva, J. M. Rautiainen, X. Ding and M. Haukka, *J. Solid State Chem.*, 2021, **295**, 121930.
18 T. I. Madzhidov, G. A. Chmutova and Á. Martín Pendás, *J. Phys. Chem. A*, 2011, **115**, 10069–10077.
19 Y. Le Gal, A. Colas, F. Barrière, V. Dorcet, T. Roisnel and D. Lorcy, *CrystEngComm*, 2019, **21**, 1934–1939.
20 C. Laurence and J.-F. Gal, in *Lewis Basicity and Affinity Scales*, ed. C. Laurence and J.-F. Gal, John Wiley & Sons, Ltd, 2009, pp. 229–321, DOI: **10.1002/9780470681909.ch5**.
21 V. Oliveira, E. Kraka and D. Cremer, *Phys. Chem. Chem. Phys.*, 2016, **18**, 33031–33046.
22 Y. Xu, J. Huang, B. Gabidullin and D. L. Bryce, *Chem. Commun.*, 2018, **54**, 11041–11043.
23 D. N. Zheng, P. M. J. Szell, S. Khiri, J. S. Ovens and D. L. Bryce, *Acta Crystallogr., Sect. B*, 2022, **78**, 557–563.
24 A. M. Siegfried, H. D. Arman, K. Kobra, K. Liu, A. J. Peloquin, C. D. McMillen, T. Hanks and W. T. Pennington, *Cryst. Growth Des.*, 2020, **20**, 7460–7469.
25 D. Hauchecorne and W. A. Herrebout, *J. Phys. Chem. A*, 2013, **117**, 11548–11557.
26 Y. Geboes, F. De Proft and W. A. Herrebout, *J. Phys. Chem. A*, 2015, **119**, 5597–5606.
27 N. M. Kreienborg, F. Otte, C. Strohmann and C. Merten, *Phys. Chem. Chem. Phys.*, 2023, **25**, 15110–15114.
28 M. Feßner, J. Bloino and C. Merten, *Phys. Chem. Chem. Phys.*, 2025, **27**, 8377–8384.
29 S. Grimme, S. Ehrlich and L. Goerigk, *J. Comput. Chem.*, 2011, **32**, 1456–1465.
30 G. Santra, N. Sylvetsky and J. M. L. Martin, *J. Phys. Chem. A*, 2019, **123**, 5129–5143.
31 O. b Shawkataly, M. A. A. Pankhi, I. A. Khan, C. S. Yeap and H.-K. Fun, *Acta Crystallogr., Sect. E*, 2009, **65**, o1525–o1526.
32 N. P. Taylor, J. A. Gonzalez, G. S. Nichol, A. García-Domínguez, A. G. Leach and G. C. Lloyd-Jones, *J. Org. Chem.*, 2022, **87**, 721–729.
33 V. R. Landaeta, F. López-Linares, R. Sánchez-Delgado, C. Bianchini, F. Zanobini and M. Peruzzini, *J. Mol. Catal. A: Chem.*, 2009, **301**, 1–10.
34 G. Nemeth, A. A. Pinkerton, J. A. Stowe and C. A. Ogle, *Acta Crystallogr., Sect. C*, 1992, **48**, 2200–2203.
35 K. R. Dunbar and S. C. Haefner, *Polyhedron*, 1994, **13**, 727–736.
36 J. A. Werra, K. Wurst, L. B. Wilm, P. Löwe, M. B. Röthel and F. Dielmann, *Organometallics*, 2023, **42**, 597–605.